

Nonlinear sloshing and passage through resonance in a shallow water tank

E. A. Cox, J. P. Gleeson and M. P. Mortell

Abstract. This paper is concerned with the effect of slowly changing the length of a tank on the nonlinear standing waves (free vibrations) and resonant forced oscillations of shallow water in the tank. The analysis begins with the Boussinesq equations. These are reduced to a nonlinear differential-difference equation for the slow variation of a Riemann invariant on one end. Then a multiple scale expansion yields a KdV equation with slowly changing coefficients for the standing wave problem, which is reduced to a KdV equation with a variable dispersion coefficient. The effect of changing the tank length on the number of solitons in the tank is investigated through numerical solutions of the variable coefficient KdV equation. A KdV equation which is “periodically” forced and slowly detuned results for the passage through resonance problem. Then the amplitude-frequency curves for the fundamental resonance and the first overtone are given numerically, as well as solutions corresponding to multiple equilibria. The evolution between multiple equilibria is also examined.

Keywords. KdV, variable coefficients, nonlinear resonance, evolution.

1. Introduction

Chester and Bones [4] performed a series of experiments involving the resonant forcing of shallow water in a tank. They showed that for sufficiently large detuning from resonance linear inviscid theory gives an adequate description of the surface motion. In the neighbourhood of resonance, however, they found that the surface motion involved relatively large amplitude peaks where the number of peaks in a period was related to the detuning. They also gave an amplitude-frequency diagram which showed the existence of multiple equilibria near resonance. Chester [3] gave a theory which described the observed periodic motions and the amplitude-frequency diagram. Cox and Mortell [5, 6] showed that the evolution of the motions from rest was governed by a periodically forced KdV equation, and they explained the observed ‘beating’ phenomena as well as showing how to evolve to the different periodic motions and to different stable equilibria at the same frequency. In a related paper, Amundsen et al. [1] considered the evolution of sloshing motions near half the fundamental frequency.

In this paper, we derive an equation which describes how the surface displacement of the shallow water is affected as the length of the tank is slowly increased or decreased. Thus, we examine first the slow change of a nonlinear “standing” wave, or free oscillation, in the tank. This is an extension of the work in Mortell [11]. We also consider the effect of the slowly changing tank length on resonantly forced oscillations and thus examine the “passage through resonance” in the tank. As a consequence we construct the amplitude-frequency diagram, the hysteresis loops, and the stable equilibrium solutions associated with those loops which exist for the same forcing frequency. We also examine the effect of diffusion damping on the equilibria and the evolution between equilibria.

The single equation which describes these resonant phenomena is a KdV equation which is ‘periodically’ forced but whose frequency changes slowly. We derive this equation using a perturbation technique on the Boussinesq equations to yield a nonlinear differential-difference equation (d.d.e.) which describes the evolution of a ‘Riemann invariant’ on the moving end of the tank. The nonlinear d.d.e. is then reduced to a partial differential equation - the forced KdV. The techniques and ideas used are an extension of those in Cox et al [7], which dealt with the case of a polytropic gas. In the case of a gas, the response curve is single-valued and there is a unique solution for a given frequency. In contrast, for water waves the periodic solutions depend on the initial conditions.

In Section 2, the Boussinesq equations are formulated in Lagrangian variables, and an initial-boundary value problem is set up for the water surface motion in a tank of changing length. The derivation of the equations for the evolution of a nonlinear “standing wave” from some initial condition is detailed in Section 3. This involves a perturbation expansion, which leads to a nonlinear differential-difference equation (d.d.e.) to determine the signal on the slowly moving boundary. A multiple-scale expansion then reduces the d.d.e. to a partial differential equation, which turns out to be the KdV equation with slowly varying coefficients. Using numerical methods, we examine the effect of the slowly changing tank length on the well-known Zabusky-Kruskal [17] soliton solutions.

In Section 4, we turn to the passage through resonance problem, where superposed on the slow motion is a fast resonant, or near resonant, oscillation. In this case, we show that the governing partial differential equation is a KdV equation subject to a resonant periodic forcing which is slowly detuned by the changing tank length. In the numerical results we find the response curves, the hysteresis loops near the first and second resonant frequencies, and the various periodic oscillations associated with these. These are in agreement with the observations of Chester and Bones [4]. New solutions, showing the effects of diffusion, are also given.

The essence of our procedure, which follows Mortell and Varley [12] and Seymour and Mortell [14], is to focus on the appropriate approximation to the travel time in the tank of the amplitudes in the signal. It is then necessary to approximate the travel time by the linear travel time plus the first nonlinear correction,

which makes the travel time dependent on the signal amplitude. Specialising to a small rate theory, see [14], allows the nonlinear d.d.e. to be reduced to a partial differential equation.

The only other works, of which we are aware, which examine passage through resonance in a continuum, and thus require a formulation in terms of a partial differential equation in contrast to an ordinary differential equation, are Steinruck [15] and Cox et al [7] where the case of a gas in a tube is considered. The interested reader will find an extensive list of references on liquid sloshing in [8]; many of the references given here complement those in [8].

2. Formulation

A tank of length L contains water of an undisturbed depth h_0 . One end of the tank is fixed, while at the other end there is a moving wave-maker. The water is shallow in the sense that $h_0/L \ll 1$. We consider disturbances, induced by the wave-maker, which have nonlinear effects of relative order a/h_0 , where a is a typical amplitude, and dispersive effects of relative order $(h_0/L)^2$. Then the Boussinesq equations, in Eulerian coordinates x , which govern the flow in the tank are, see Whitham [16],

$$\frac{\partial h}{\partial t} + \frac{\partial}{\partial x}(uh) = 0, \quad (1)$$

$$\frac{\partial u}{\partial t} + u \frac{\partial u}{\partial x} + g \frac{\partial h}{\partial x} + \frac{1}{3} h_0 \frac{\partial^3 h}{\partial x \partial t^2} = 0. \quad (2)$$

The equations used in Chester [3], when the dissipative term is neglected, are a variant of the Boussinesq equations, but greater accuracy is not claimed for these. In (1), (2), $h(x, t)$ is the height of the water, $u(x, t)$ is the horizontal velocity, and g is the acceleration due to gravity.

We take h_0 as the unit of height, $c_0 = (gh_0)^{1/2}$ as the unit of velocity, L as the unit of length, Lc_0^{-1} as the unit of time, and denote dimensionless quantities with a bar. We let $\bar{h}(x, t) = 1 + \eta(\bar{x}, \bar{t})$, so that $\eta(\bar{x}, \bar{t})$ is the (nondimensional) surface displacement from the undisturbed height, and then (1) and (2) imply

$$\eta_{\bar{t}} + [(1 + \eta)\bar{u}]_{\bar{x}} = 0, \quad (3)$$

$$\bar{u}_{\bar{t}} + \bar{u}\bar{u}_{\bar{x}} + \eta_{\bar{x}} + \frac{1}{3}\delta^2\eta_{\bar{x}\bar{t}\bar{t}} = 0, \quad (4)$$

where $\delta = h_0/L \ll 1$ is the dimensionless parameter associated with frequency dispersion. We note that for $\delta = 0$, (3), (4) are the equations for a polytropic gas with $\gamma = 2$ – the “gas dynamics” analogy, or hydraulic flow.

We define the Lagrangian variable X by

$$X = \int_0^{\bar{x}} [1 + \eta(s, \bar{t})] ds, \quad 0 \leq \bar{x} \leq \bar{x}_p(\bar{t}), \quad (5)$$

where $\bar{x}_p(\bar{t})$ is the position of the wave-maker. Then we have $0 \leq X \leq 1$, where the wave-maker is at $X = 1$. A new dependent variable $P(X, \bar{t})$ is introduced by

$$P(X, \bar{t}) = [1 + \eta(X, \bar{t})]^{1/2}. \quad (6)$$

On transforming (3), (4) to Lagrangian variables, using the transformation (6), and writing the resulting equations in characteristic form, we have to the same order as (3) and (4),

$$\frac{\partial}{\partial \alpha} \left(\frac{\bar{u}}{2} + P \right) = -\frac{1}{3} \delta^2 \frac{\partial^3 P}{\partial X \partial \bar{t}^2}, \quad \frac{\partial X}{\partial \alpha} = P^3 \frac{\partial \bar{t}}{\partial \alpha}, \quad (7)$$

$$\frac{\partial}{\partial \beta} \left(\frac{\bar{u}}{2} - P \right) = -\frac{1}{3} \delta^2 \frac{\partial^3 P}{\partial X \partial \bar{t}^2}, \quad \frac{\partial X}{\partial \beta} = -P^3 \frac{\partial \bar{t}}{\partial \beta}. \quad (8)$$

When $\delta = 0$, these are the polytropic gas equations in Cox et al. [7] when the gas constant $\gamma = 2$. Then, of course, $\frac{\bar{u}}{2} + P$ and $\frac{\bar{u}}{2} - P$ in (7) and (8) are just the Riemann Invariants. We note that the introduction of the transformation (6) yields linear transport equations and nonlinear characteristic equations in (7) and (8).

The wave-maker at $X = 1$ can induce a ‘slow’ expansion or contraction in the length of the tank, and superimposed on this can be a ‘fast’ small amplitude, fixed frequency oscillation. The wave-maker displacement may thus be written

$$X_p(\bar{t}) = \tilde{X}_p(\epsilon \bar{t}) + \epsilon \tilde{v}(\omega \bar{t}), \quad (9)$$

where $\tilde{X}_p(\epsilon \bar{t})$ is the slow mean displacement of the wave-maker, \tilde{v} is a periodic function with unit period in $\omega \bar{t}$, and $\epsilon \ll 1$ is the ratio of the maximum oscillatory displacement about the mean to the initial tank length $\tilde{X}_p(0) = L$. Further, ω^{-1} is the non-dimensional period of the wave-maker about its slowly moving mean position. The boundary condition at $X = 1$ now is

$$\bar{u}(1, \bar{t}) = \epsilon \tilde{X}_p'(\epsilon \bar{t}) + v(\omega \bar{t}), \quad \bar{t} > 0, \quad (10)$$

where $v(\omega \bar{t}) = \epsilon \omega \tilde{v}'(\omega \bar{t})$ – hence has zero mean over one period – and the prime denotes differentiation with respect to the argument shown. The boundary condition at the fixed end $X = 0$ is

$$\bar{u}(0, \bar{t}) = 0. \quad (11)$$

We consider two problems here: (i) the evolution of a ‘standing’ wave, when $v \equiv 0$ in (10), and the motion of the water arises from an initial disturbance while the tank itself is being slowly lengthened or shortened by changing the position of the wave-maker; (ii) the behaviour of the surface elevation under excitation by a resonant piston motion which is being slowly detuned due to the changing mean position of the wave-maker. We refer to this latter case as ‘passage through resonance’.

In the case of the standing wave, we will follow the evolution from an initial state; for the resonant motion we will confine our attention to passage through the resonant band. These nonlinear initial-boundary value problems on a semi-infinite

strip are completely specified by (6), (7), (8), (10), (11), and the specification of $\bar{u}(X, \bar{t})$ and $\eta(X, \bar{t})$ on $0 \leq X \leq 1$ for $\bar{t} \leq 0$.

3. Evolution of nonlinear standing wave

We consider the case when $v \equiv 0$ in (10), and (11) holds, i.e., $\bar{u}(1, \bar{t}) = \epsilon \tilde{X}'_p(\epsilon \bar{t})$, which corresponds to a ‘slow’ movement of the wave-maker in or out of the tank. The amplitude of the initial disturbance is $O(\epsilon) \ll 1$. We expand the resulting motion of the water in the form

$$P(\alpha, \beta) = 1 + P_0(\sigma) + \epsilon P_1(\alpha, \beta) + \epsilon^2 P_2(\alpha, \beta) + \dots, \tag{12}$$

$$\bar{u}(\alpha, \beta) = \epsilon u_1(\alpha, \beta) + \epsilon^2 u_2(\alpha, \beta) + \dots, \tag{13}$$

where

$$\sigma = \frac{1}{2}\epsilon(\alpha + \beta) \tag{14}$$

is a slow time scale. The term $P_0(\sigma)$ in (12) accounts from the slow change in the mean depth, while the other terms account for the fast motion induced by the initial conditions. The characteristic equations in (7), (8) are expanded as

$$X(\alpha, \beta; \epsilon) = X_0(\alpha, \beta) + \epsilon X_1(\alpha, \beta) + \dots \tag{15}$$

$$\bar{t}(\alpha, \beta; \epsilon) = t_0(\alpha, \beta) + \epsilon t_1(\alpha, \beta) + \dots, \tag{16}$$

which is essentially Lin’s technique [10]. On substituting (12), (13), (15) and (16) into (7) and (8), and noting (14), we get the following sequence of equations.

$$\frac{\partial}{\partial \alpha} \left(P_1 + \frac{u_1}{2} \right) + \frac{1}{2} P'_0(\sigma) = 0, \tag{17}$$

$$\frac{\partial}{\partial \beta} \left(P_1 - \frac{u_1}{2} \right) + \frac{1}{2} P'_0(\sigma) = 0, \tag{18}$$

$$\frac{\partial X_0}{\partial \alpha} - [1 + P_0(\sigma)]^3 \frac{\partial t_0}{\partial \alpha} = 0, \tag{19}$$

$$\frac{\partial X_0}{\partial \beta} + [1 + P_0(\sigma)]^3 \frac{\partial t_0}{\partial \beta} = 0. \tag{20}$$

Solutions are

$$P_1 = f(\alpha) + g(\beta), \tag{21}$$

$$u_1 = 2g(\beta) - 2f(\alpha) - (\alpha - \beta)P'_0(\sigma), \tag{22}$$

with

$$X_0 = \frac{1}{2}(\alpha - \beta), \quad t_0 = \epsilon^{-1} \int_{\epsilon}^{\frac{1}{2}\epsilon(\alpha+\beta)} [1 + P_0(s)]^{-3} ds. \tag{23}$$

It should be noted that the form of t_0 in (23) allows for the fact that the mean depth is changing, and hence the wave speed in the water is changing. Effectively, the medium is becoming inhomogeneous since the wave speed is changing slowly.

At the next order, the equations for u_2, P_2 are

$$\begin{aligned} \frac{\partial}{\partial \alpha} \left(\frac{u_2}{2} + P_2 \right) &= -\frac{\kappa}{3} (1 + P_0(\sigma))^6 \left(\frac{\partial}{\partial \alpha} + \frac{\partial}{\partial \beta} \right)^2 \left(\frac{\partial}{\partial \alpha} - \frac{\partial}{\partial \beta} \right) P_1 \\ &\quad - \frac{1}{2} \frac{\partial}{\partial \sigma} \left(\frac{u_1}{2} + P_1 \right), \end{aligned} \tag{24}$$

$$\begin{aligned} \frac{\partial}{\partial \beta} \left(\frac{u_2}{2} - P_2 \right) &= -\frac{\kappa}{3} (1 + P_0(\sigma))^6 \left(\frac{\partial}{\partial \alpha} + \frac{\partial}{\partial \beta} \right)^2 \left(\frac{\partial}{\partial \alpha} - \frac{\partial}{\partial \beta} \right) P_1 \\ &\quad - \frac{1}{2} \frac{\partial}{\partial \sigma} \left(\frac{u_1}{2} - P_1 \right), \end{aligned} \tag{25}$$

where

$$\delta^2 = \kappa \epsilon, \quad \kappa = O(1). \tag{26}$$

An approximate solution for u_2 , neglecting terms of higher order, is

$$u_2 = \frac{\kappa}{3} (1 + P_0(\sigma))^6 [g''(\beta) - f''(\alpha) - (\beta - \alpha) \{f'''(\alpha) + g'''(\beta)\}] + 2g_2(\beta) - 2f_2(\alpha), \tag{27}$$

where $g_2(\beta), f_2(\alpha)$ are solutions of the homogeneous form of equations (24), (25) respectively.

The equations for X_1, t_1 are

$$\frac{\partial X_1}{\partial \alpha} - [1 + P_0(\sigma)]^3 \frac{\partial t_1}{\partial \alpha} = 3 [1 + P_0(\sigma)]^2 P_1 \frac{\partial t_0}{\partial \alpha}, \tag{28}$$

and

$$\frac{\partial X_1}{\partial \beta} + [1 + P_0(\sigma)]^3 \frac{\partial t_1}{\partial \beta} = -3 [1 + P_0(\sigma)]^2 P_1 \frac{\partial t_0}{\partial \beta}, \tag{29}$$

with solutions

$$X_1 - [1 + P_0(\sigma)]^3 t_1 = \frac{3}{2 [1 + P_0(\sigma)]} \left[(\alpha - \beta)g(\beta) + \int_{\beta}^{\alpha} f(s)ds \right] \tag{30}$$

and

$$X_1 + [1 + P_0(\sigma)]^3 t_1 = \frac{3}{2 [1 + P_0(\sigma)]} \left[(\alpha - \beta)f(\alpha) + \int_{\beta}^{\alpha} g(s)ds \right]. \tag{31}$$

We see from (23), (30), (31) that $\alpha = \beta$ implies $X = X_0 + \epsilon X_1 = 0$. Then, using (22) and (27), the boundary condition (11) on $X = 0$ in the form $\bar{u} = \epsilon u_1 + \epsilon^2 u_2 = 0$ implies $f = g$ and $f_2 = g_2$. The boundary condition

$$\epsilon u_1 + \epsilon^2 u_2 = \epsilon \tilde{X}'_p(\epsilon \bar{t})$$

on $X = 1$ then implies, using (22) and (27),

$$\begin{aligned} f(\beta) - f(\alpha) - \frac{1}{2}(\alpha - \beta)P'_0(\sigma) \\ + \frac{\kappa \epsilon}{6} (1 + P_0(\sigma))^6 [f''(\beta) - f''(\alpha) - (\beta - \alpha) \{f'''(\alpha) + f'''(\beta)\}] = U_p(\epsilon \bar{t}), \end{aligned} \tag{32}$$

where $U_p(\epsilon\bar{t}) = \tilde{X}'_p(\epsilon\bar{t})$ in (10). In deriving (32), we have incorporated f_2 into the, at this stage arbitrary, f .

Similarly, $X_0 + \epsilon X_1 = 1$, on using (23), (30) and (31), implies

$$1 = \frac{1}{2}(\alpha - \beta) + \frac{3\epsilon}{4[1 + P_0(\sigma)]} \left[(\alpha - \beta) \{f(\alpha) + f(\beta)\} + 2 \int_{\beta}^{\alpha} f(s) ds \right]. \quad (33)$$

Thus α and β in (32) are connected by the relation (33). It might be noted that the idea of satisfying the boundary conditions at two orders simultaneously is in the spirit of Chester [3] and Cox and Mortell [6]. We refer to (32) and (33) as a *nonlinear differential-difference* equation for the unknown signal f on $X = 1$. We note that the difference, or travel time, $(\alpha - \beta)$ depends on the unknown f . Once f on $X = 1$ is determined, $\bar{u}(1, \bar{t})$ and $\eta(1, \bar{t})$ are found from (6), (12), (13), (21), (22), since $g = f$. Then the relations (23) allow $\eta(X, \bar{t})$ to be calculated from $\eta(1, \bar{t})$. Even though they are in differential-difference form, equations (32) and (33) are the *transport* and *characteristic* equations, respectively.

We can relate the rate of change of mean depth to the imposed slow piston motion through

$$P'_0(\sigma) = -U_p(\epsilon\bar{t}), \quad (34)$$

see Steinruck [15], Cox et al [7], which integrates to

$$1 + P_0(\sigma) = \left[\tilde{X}_p(\epsilon\bar{t}) \right]^{-\frac{1}{2}}. \quad (35)$$

By (12) and (6), we can see that (35) is just a statement of conservation of mass: $(1 + \eta)\tilde{X}_p = 1$. Equation (34) can also be derived as a secularity condition on P_0 to ensure P_1 is bounded, see Klein and Peters [9] for a similar result in the context of gas dynamics.

We iterate on (33) and introduce $F = 6f$; then the relationship between α and β on $X = 1$ becomes to $O(\epsilon^2)$,

$$\alpha = \beta + 2 - \frac{\epsilon}{1 + P_0(\sigma)} \left[F(\beta) + \frac{1}{2} \int_{\beta}^{\beta+2} F(s) ds \right]. \quad (36)$$

On using (34), the transport equation (32) becomes, to $O(\epsilon^2)$,

$$F(\alpha) = F(\beta) - 3(\alpha - \beta - 2)P'_0(\sigma) + \frac{1}{6}\kappa\epsilon(1 + P_0(\sigma))^6 [F''(\beta) - F''(\alpha) + 2(F'''(\alpha) + F'''(\beta))]. \quad (37)$$

We note, in passing, that since our expansions have assumed that F', F'', F''' are all the same order as F , we are implicitly working with a small rate theory, see Seymour and Mortell [14].

In order to solve the nonlinear differential-difference equations (36) and (37), we use a two-variable expansion scheme, Cox and Mortell [5]. By (36),

$$F(\alpha) = F(\beta + 2) - \frac{\epsilon}{1 + P_0(\sigma)} \left[F(\beta) + \frac{1}{2} \int_{\beta}^{\beta+2} F(s) ds \right] F'(\beta + 2) + O(\epsilon^2). \quad (38)$$

Equating $F(\alpha)$ in (37) and (38), and using (36), we find to $O(\epsilon^2)$

$$\begin{aligned}
 F(\beta + 2) = & F(\beta) + \frac{\epsilon}{1 + P_0(\sigma)} \left[F(\beta) + \frac{1}{2} \int_{\beta}^{\beta+2} F(s) ds \right] [3P'_0(\sigma) + F'(\beta + 2)] \\
 & + \frac{1}{6} \kappa \epsilon (1 + P_0(\sigma))^6 [F''(\beta) - F''(\alpha) + 2(F'''(\alpha) + F'''(\beta))]. \quad (39)
 \end{aligned}$$

We introduce a slow variable by $\tau = \epsilon\beta/2$, and note that on $X = 1$, $\sigma = 2\tau + \epsilon + O(\epsilon^2)$. We assume the expansion

$$F(\beta; \epsilon) = F_0(\beta, \tau) + \epsilon F_1(\beta, \tau) + \dots, \quad (40)$$

and substitute into (39). At first order we have

$$F_0(\beta + 2, \tau) = F_0(\beta, \tau), \quad (41)$$

and a bounded solution at next order requires that F_0 evolves according to

$$\begin{aligned}
 \frac{\partial F_0}{\partial \tau} - \frac{1}{1 + \hat{P}_0(\tau)} [F_0 + M_0(\tau)] \frac{\partial F_0}{\partial \beta} \\
 - \frac{3\hat{P}'_0(\tau)}{2[1 + \hat{P}_0(\tau)]} F_0 - \frac{\kappa}{3} [1 + \hat{P}_0(\tau)]^6 \frac{\partial^3 F_0}{\partial \beta^3} = \frac{3\hat{P}'_0(\tau)}{2[1 + \hat{P}_0(\tau)]} M_0(\tau), \quad (42)
 \end{aligned}$$

where

$$M_0(\tau) = \frac{1}{2} \int_{\beta}^{\beta+2} F_0(s, \tau) ds \quad (43)$$

is the mean of F_0 over one cycle. By (41), $F_0(\beta, \tau)$ is a free vibration or a “standing wave” modulated on the time scale associated with τ . The evolution of the signal carried by the “standing wave” is determined by (42) from the given initial condition. We have written $P_0(\sigma)|_{X=1} \equiv \hat{P}_0(\tau)$. We note that if $\hat{P}_0(\tau) = 0$ (thus $U_p \equiv 0$) and $M_0(\tau) = 0$, (42) is the KdV equation.

The term $M_0(\tau)$ in (42) arises from the interaction of oppositely travelling waves; the term involving $\hat{P}'_0(\tau)$ on the left hand side of (42), which by (34) arises directly from the mean velocity of the wave-maker, gives rise to attenuation ($\hat{P}' < 0$) or amplification ($\hat{P}' > 0$) of the signal F_0 . When (42) is integrated with respect to β over one cycle, the mean of the standing wave, $M_0(\tau)$, is given by

$$M_0(\tau) = M_0(0) [1 + \hat{P}_0(\tau)]^3. \quad (44)$$

Thus if $M_0(0) = 0$, i.e., the initial condition on F has zero mean, then $M_0(\tau) = 0$ and the mean of F remains zero throughout the evolution. Finally, we note that if $\kappa = 0$, (42) describes hydraulic flow in a tank and can be integrated exactly, see Cox et al [7].

3.1. Numerical results

We consider an initial state with mean zero, i.e., $M_0(\tau) = 0$ in (42), and introduce the transformations

$$c(\tau) = 1 + \hat{P}_0(\tau), \quad H(\beta, \tau) = c^{-3/2} F_0(\beta, \tau), \quad \hat{\tau} = \int_0^\tau c^{1/2}(s) ds. \quad (45)$$

Then (42) becomes

$$\frac{\partial H}{\partial \hat{\tau}} - H \frac{\partial H}{\partial \beta} - \kappa(\hat{\tau}) \frac{\partial^3 H}{\partial \beta^3} = 0, \quad (46)$$

where

$$\kappa(\hat{\tau}) = \frac{1}{6} \kappa c^{\frac{11}{2}}(\hat{\tau}). \quad (47)$$

If we take a piston displacement

$$X_p(\epsilon \bar{t}) = 1 - \epsilon \bar{t}, \quad (48)$$

then, on $X = 1$, $c(\tau) = 1 + \tau$ and

$$c(\hat{\tau}) = \left(1 + \frac{3}{2} \hat{\tau}\right)^{2/3},$$

so

$$\kappa(\hat{\tau}) = \frac{1}{6} \kappa \left(1 + \frac{3}{2} \hat{\tau}\right)^{11/3}. \quad (49)$$

The dispersion $\kappa(\hat{\tau})$ is a function of the slow variable reflecting the fact that the tank length is increasing or decreasing, and thus the mean depth of water is decreasing or increasing. We require the periodicity condition $H(\beta + 2, \hat{\tau}) = H(\beta, \hat{\tau})$, and take as initial condition $H(\beta, 0) = a \cos(\pi\beta)$. When the dispersion coefficient $\kappa(\hat{\tau})$ is a constant κ , (46) is a Korteweg-deVries (KdV) equation with periodic boundary conditions. As shown by Zabusky and Kruskal [17], solutions consisting of a number of solitons may exist. Indeed, the formula

$$N = 0.88 \left(\frac{a}{2\pi^2 \kappa}\right)^{1/2} \quad (50)$$

has been proposed [13] to give the number of solitons N resulting from the solution of (46) with constant dispersion $\kappa(\hat{\tau}) = \kappa$. It may be supposed that the formula (50) holds when the dispersion coefficient changes slowly in time, i.e. if the piston motion is slow. Our goal in this section is to investigate this hypothesis using numerical solutions of (46). We choose the values of the initial amplitude $a = 0.1$ and initial dispersion $\kappa = 9.8 \times 10^{-4}$ to give $N = 2$ from formula (50), and consider changing the dispersion coefficient over time to a lower value of $\kappa_1 = \frac{4}{9} \kappa = 4.356 \times 10^{-4}$. When the dispersion has this lower value, (50) predicts exactly three solitons should co-exist in the tank.

We begin by examining the two-soliton solution, taking the dispersion $\kappa(\hat{\tau})$ to have the constant value κ . To track the solitons, the positions of local maxima

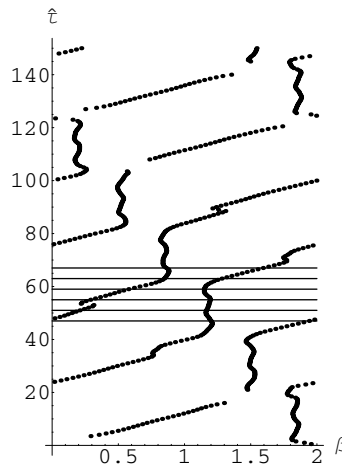


Figure 1. β - $\hat{\tau}$ diagram showing soliton peaks. Dispersion is constant $\kappa(\hat{\tau}) = \kappa$. Horizontal lines mark the profile snapshots of Figure 2.

of the solution profile $H(\beta, \hat{\tau})$ are marked at each time $\hat{\tau}$ on the β - $\hat{\tau}$ diagram of Figure 1. The horizontal axis gives the β value, with $\hat{\tau}$ increasing from 0 to 150 along the vertical axis. There are two local maxima at each timestep, tracking the peaks of the expected two solitons. A certain periodicity in $\hat{\tau}$ is evident from Figure 1, which is due to the approximate recurrence (with phase-shifts) of the combination of solitons. We show in Figure 2 the solution profiles $H(\beta, \hat{\tau})$ as a function of β at six values of $\hat{\tau}$, corresponding to the horizontal lines on Figure 1. Beginning at $\hat{\tau} = 47$ with two solitons, the motion of each may be followed through times $\hat{\tau} = 51$, $\hat{\tau} = 55$, $\hat{\tau} = 59$, $\hat{\tau} = 63$, until at $\hat{\tau} = 67$ we have a configuration very close to that at $\hat{\tau} = 47$, but shifted in β .

Next we consider the changes observed when the effective dispersion coefficient $\kappa(\hat{\tau})$ changes, due to the piston motion altering the tank length. When the piston is pulled out at a constant speed, starting at time $\hat{\tau}_1$ and stopping at time $\hat{\tau}_2$, the piston position is

$$X_p = 1 + \delta(\hat{\tau} - \hat{\tau}_1)$$

for $\hat{\tau}_1 < \hat{\tau} < \hat{\tau}_2$. As a result, the effective dispersion decreases from κ to

$$\kappa(\hat{\tau}) = \kappa \left(1 - \frac{3}{2} \delta(\hat{\tau} - \hat{\tau}_1) \right)^{11/3} \quad (51)$$

over the same time interval. We choose the duration $\hat{\tau}_2 - \hat{\tau}_1$ of the piston motion to ensure that the effective dispersion value is $\kappa_1 = 4\kappa/9$ when the piston stops moving. If we now continue to evolve the solution with this new constant dispersion value κ_1 , formula (50) predicts precisely three solitons in the tank. Taking the

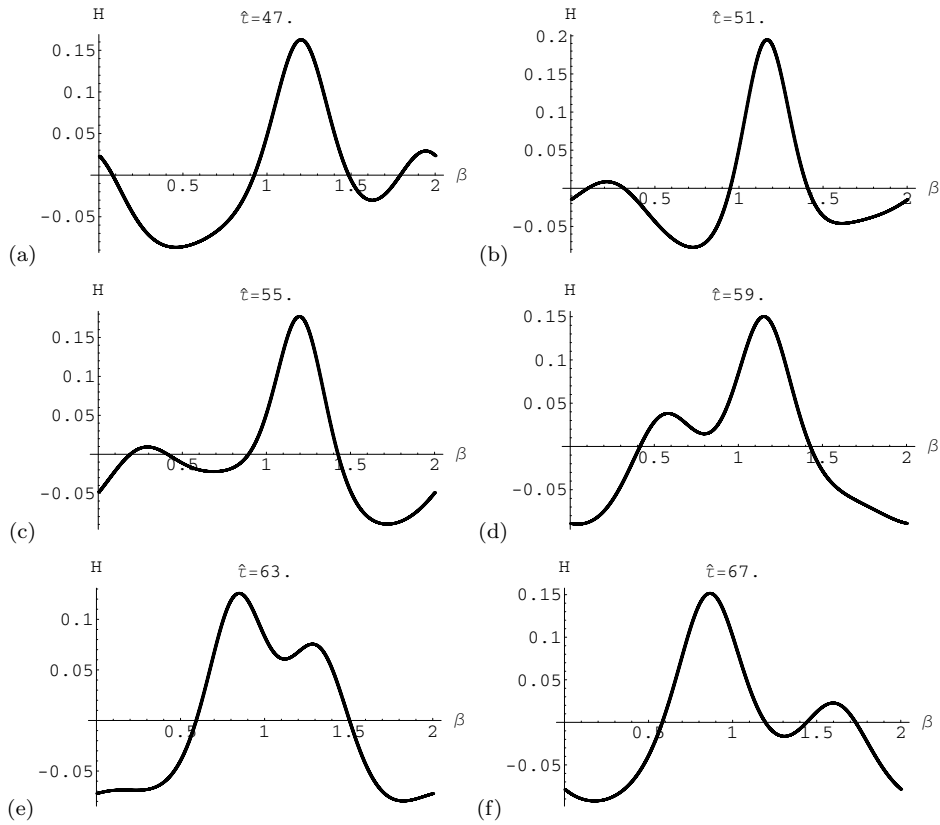


Figure 2. Solution profiles $H(\beta, \hat{\tau})$ corresponding to Figure 1 at: (a) $\hat{\tau} = 47$, (b) $\hat{\tau} = 51$, (c) $\hat{\tau} = 55$, (d) $\hat{\tau} = 59$, (e) $\hat{\tau} = 63$, (f) $\hat{\tau} = 67$.

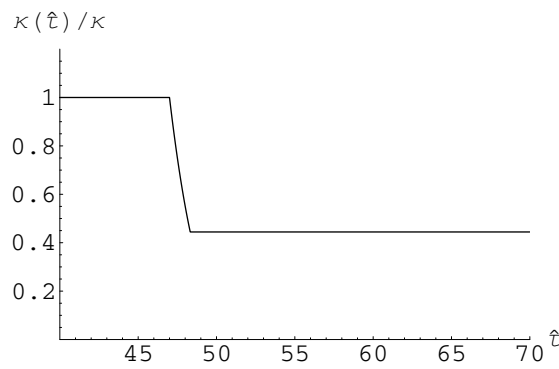


Figure 3. The effective dispersion $\kappa(\hat{\tau})/\kappa$ as a function of $\hat{\tau}$ due to pulling piston out at speed $\delta = 0.1$, starting at $\hat{\tau}_1 = 47$, and stopping at $\hat{\tau}_2 = 48.3228$.

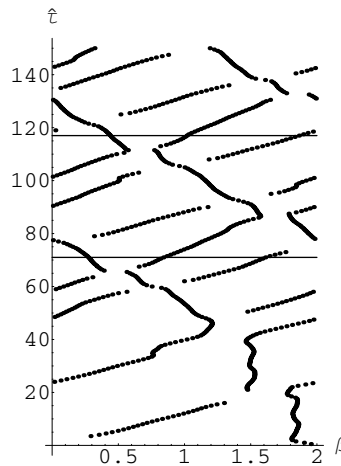


Figure 4. β - $\hat{\tau}$ diagram showing soliton peaks for the effective dispersion of Figure 3.

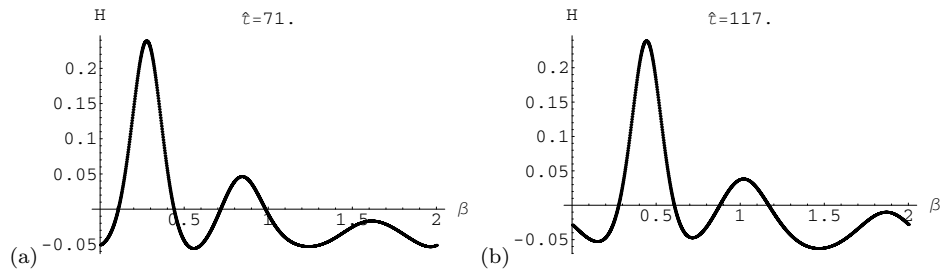


Figure 5. Solution profiles $H(\beta, \hat{\tau})$ corresponding to Figure 4 at: (a) $\hat{\tau} = 71$, (b) $\hat{\tau} = 117$.

speed δ of the piston motion to be 0.1, and beginning the motion at $\hat{\tau}_1 = 47$, Figure 3 shows the effective dispersion normalized by κ . The resulting β - $\hat{\tau}$ tracks of the solitons are shown in Figure 4. Note that up until the piston is moved at $\hat{\tau} = \hat{\tau}_1 = 47$ the tracks match those in Figure 1. However, the change in dispersion resulting from the piston motion at $\hat{\tau} = \hat{\tau}_1$ soon leads to the development of a third soliton. The three solitons settle into a new pattern of almost-recurrence; note the repetition of the pattern between the horizontal lines in Figure 4. The profiles at $\hat{\tau} = 71$ and $\hat{\tau} = 117$ (Figure 5) clearly show the three solitons, and demonstrate the phase-shifted recurrence.

The process of formation of the new soliton is shown in greater detail in Figure 6, where solution profiles are plotted from $\hat{\tau} = \hat{\tau}_1 = 47$ to $\hat{\tau} = 52$. At $\hat{\tau} = 47$, the profile is identical to that in Figure 2(a), as no change in the dispersion has yet occurred. Following the change in dispersion initiated at $\hat{\tau} = 47$, the profile

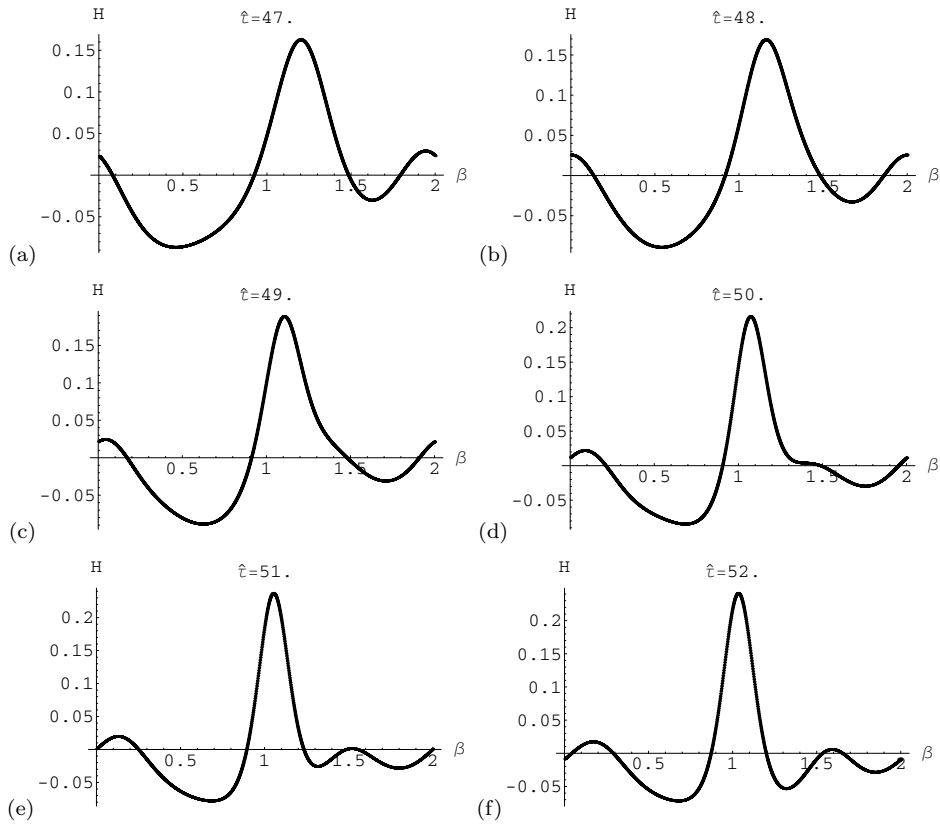


Figure 6. Solution profiles $H(\beta, \hat{\tau})$ corresponding to Figure 4 at: (a) $\hat{\tau} = 47$, (b) $\hat{\tau} = 48$, (c) $\hat{\tau} = 49$, (d) $\hat{\tau} = 50$, (e) $\hat{\tau} = 51$, (f) $\hat{\tau} = 52$.

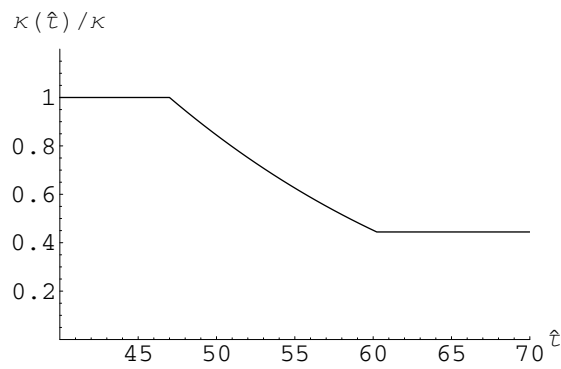


Figure 7. The effective dispersion $\kappa(\hat{\tau})/\kappa$ as a function of $\hat{\tau}$ due to pulling piston out at speed $\delta = 0.01$, starting at $\hat{\tau}_1 = 47$, and stopping at $\hat{\tau}_2 = 60.2276$.

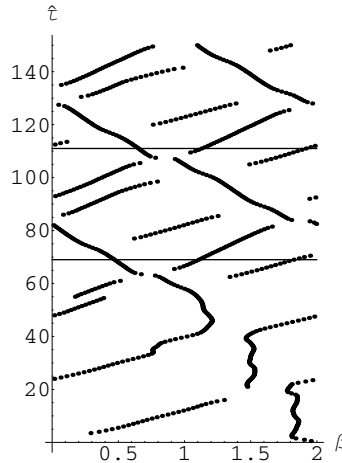


Figure 8. β - $\hat{\tau}$ diagram showing soliton peaks for the effective dispersion of Figure 7.

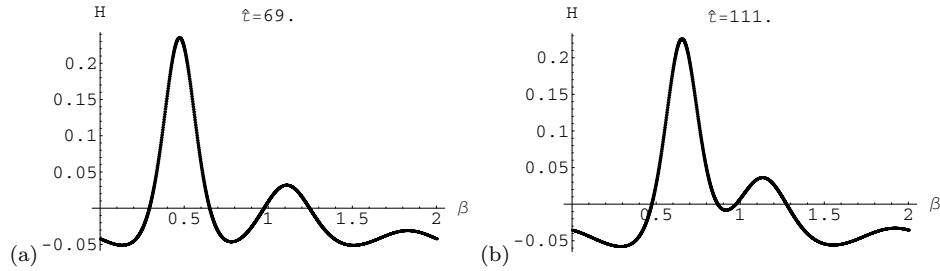


Figure 9. Solution profiles $H(\beta, \hat{\tau})$ corresponding to Figure 8 at: (a) $\hat{\tau} = 69$, (b) $\hat{\tau} = 111$.

changes from that in Figure 2, culminating in the emergence of the third soliton, clearly visible by $\hat{\tau} = 51$ (Fig. 6(e)). The new soliton appears to be formed by splitting of the larger of the original two solitons into two entities, the larger moving to the left and the smaller to the right, see Figure 4.

If we again pull the piston out, but at the slower speed of $\delta = 0.01$, we keep the piston in motion for a longer duration in order to reach the dispersion value κ_1 , see Figure 7. The results in Figure 8 are qualitatively similar to the previous case, with a third soliton forming and generating a new recurrence pattern. Note from Figure 9 that the amplitude of the third soliton is lower in this case.

Thus far our numerical experiments support the hypothesis that the formula (50) can be applied when the dispersion coefficient $\kappa(\hat{\tau})$ has reached a steady value. However, the situation is not quite that simple, as can be seen from our final experiment. Here we pull the piston out at speed $\delta = 0.01$ as in the last

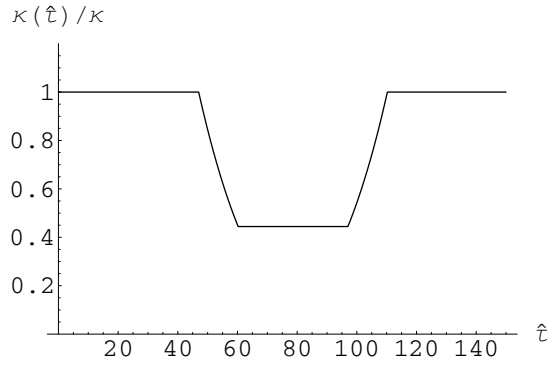


Figure 10. The effective dispersion $\kappa(\hat{\tau})/\kappa$ as a function of $\hat{\tau}$ due to pulling piston out at speed $\delta = 0.01$, from $\hat{\tau}_1 = 47$, and pushing the piston back in from $\hat{\tau}_3 = 97$.

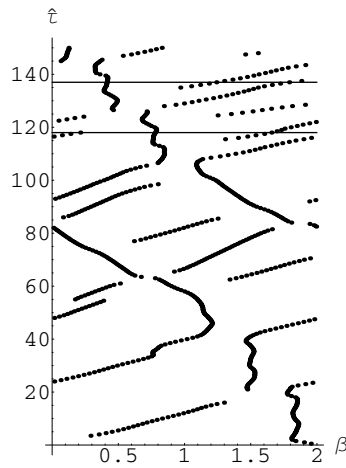


Figure 11. β - $\hat{\tau}$ diagram showing soliton peaks for the effective dispersion of Figure 10.

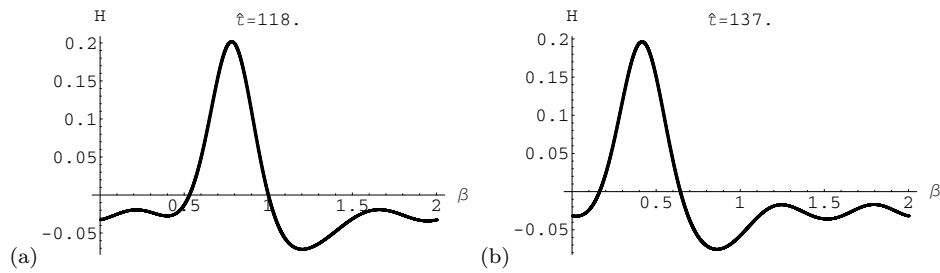


Figure 12. Solution profiles $H(\beta, \hat{\tau})$ corresponding to Figure 11: (a) $\hat{\tau} = 118$, (b) $\hat{\tau} = 137$.

example, then hold it steady for some $\hat{\tau}$ interval to allow the third soliton to form and interact. Then at time $\hat{\tau}_3 = 97$, we push the piston back in, i.e. move it with speed $\delta = -0.01$, until the effective dispersion returns to its original value of κ , see Figure 10. It might be expected that the third soliton which was formed at the lower dispersion value of κ_1 will disappear when the dispersion returns to κ , leaving just the two solitons predicted from (50). As shown in Figures 11 and 12, this is not the case; indeed the three solitons remain and appear to give a new recurrence pattern. We conclude that the soliton dynamics depend on the history of the dispersion coefficient, rather than simply on its instantaneous value $\kappa(\hat{\tau})$.

4. Passage through fundamental resonance

We now wish to examine (7) and (8) subject to the closed end condition (11), while the condition on the wave-maker at $X = 1$ is

$$\bar{u}(1, \bar{t}) = \epsilon U_p(\epsilon \bar{t}) - \Lambda \epsilon \sin(2\pi\omega \bar{t}), \quad (52)$$

where $\bar{v}(\eta) = \cos(2\pi\eta)$ in (10), $\Lambda = 2\pi\omega$, and $U_p(\epsilon \bar{t}) = \tilde{X}'_p(\epsilon \bar{t})$. Thus, by (52), as the mean velocity of the wave-maker changes ‘slowly’ (on a time scale $\epsilon \bar{t} = O(1)$), there is superposed on it a small amplitude ‘fast’ oscillation with unit period in $\omega \bar{t}$. If ω is the fundamental frequency, the mean motion of the wave-maker in lengthening or shortening the tank slowly detunes the system. In this context, we examine the passage through resonance.

When $U_p(\epsilon \bar{t}) \equiv 0$, $\bar{u}(X, \bar{t}) = O(\epsilon^{\frac{1}{2}})$ at the fundamental frequency, see Betchov [2]. Then to get the right balance between nonlinearity and frequency dispersion during the passage through resonance we require

$$\delta^2 = 4\kappa\epsilon^{\frac{1}{2}} \quad (53)$$

in (7) and (8). The expansions for $P(\alpha, \beta)$ and $\bar{u}(\alpha, \beta)$ are assumed in the form

$$P(\alpha, \beta; \epsilon) = 1 + P_0(\sigma) + \epsilon^{\frac{1}{2}}P_1(\alpha, \beta) + \epsilon P_2(\alpha, \beta) + \dots, \quad (54)$$

$$\bar{u}(\alpha, \beta; \epsilon) = \epsilon^{\frac{1}{2}}u_1(\alpha, \beta) + \epsilon u_2(\alpha, \beta) + \dots, \quad (55)$$

where

$$\sigma = \frac{\epsilon}{2\omega}(\alpha + \beta). \quad (56)$$

The governing equations (7) and (8), on using (53), become

$$\begin{aligned} 2\omega \left(\frac{\partial}{\partial \alpha} + \frac{\epsilon}{2\omega} \frac{\partial}{\partial \sigma} \right) \left(\frac{\bar{u}}{2} + P \right) &= -\frac{4}{3}\kappa\epsilon^{\frac{1}{2}} \frac{\partial^3 P}{\partial X \partial \bar{t}^2}, \\ 2\omega \left(\frac{\partial}{\partial \beta} + \frac{\epsilon}{2\omega} \frac{\partial}{\partial \sigma} \right) \left(\frac{\bar{u}}{2} - P \right) &= -\frac{4}{3}\kappa\epsilon^{\frac{1}{2}} \frac{\partial^3 P}{\partial X \partial \bar{t}^2}. \end{aligned}$$

(See the comment following equation (77)). Then the sequence of equations to be solved is

$$\left(\frac{u_1}{2} + P_1 \right)_{,\alpha} = \left(\frac{u_1}{2} - P_1 \right)_{,\beta} = 0, \quad (57)$$

and

$$2\omega \left(\frac{u_2}{2} + P_2\right)_{,\alpha} = -P'_0(\sigma) - \frac{4}{3}\omega^3\kappa [P_{1,\alpha\alpha\alpha} - P_{1,\beta\beta\beta}], \tag{58}$$

$$2\omega \left(\frac{u_2}{2} - P_2\right)_{,\beta} = P'_0(\sigma) - \frac{4}{3}\omega^3\kappa [P_{1,\alpha\alpha\alpha} - P_{1,\beta\beta\beta}], \tag{59}$$

on noting the forms of the solutions to (57).

The solutions are

$$u_1 = 2g(\beta) - 2f(\alpha), \quad P_1 = g(\beta) + f(\alpha) \tag{60}$$

and

$$2\omega \left(\frac{u_2}{2} + P_2\right) = -(\alpha - \beta)P'_0(\sigma) - \frac{4}{3}\omega^3\kappa [f''(\alpha) - (\beta - \alpha)g'''(\beta)], \tag{61}$$

$$2\omega \left(\frac{u_2}{2} - P_2\right) = -(\alpha - \beta)P'_0(\sigma) - \frac{4}{3}\omega^3\kappa [(\beta - \alpha)f'''(\alpha) - g''(\beta)]. \tag{62}$$

In (60), f and g are arbitrary functions which will be determined by the boundary and initial conditions to yield u_1 and P_1 , while (61) and (62) are particular integrals of (58) and (59) respectively. We could add an arbitrary function of β to (61) and an arbitrary function of α to (62); however these are determined at $O(\epsilon^{\frac{3}{2}})$ and add nothing to the basic solution (60).

We now expand $X(\alpha, \beta; \epsilon)$ and $\bar{t}(\alpha, \beta; \epsilon)$ in powers of $\epsilon^{\frac{1}{2}}$ and note (56). The result is a slight modification of the corresponding calculation in Section 3. The characteristic (or travel time equation) is

$$\omega = \frac{1}{2}(\alpha - \beta) + \frac{3\epsilon^{\frac{1}{2}}}{4[1 + P_0(\sigma)]} \left[(\alpha - \beta)(f(\alpha) + f(\beta)) + 2 \int_{\beta}^{\alpha} f(s)ds \right], \tag{63}$$

where $\alpha = \beta$ on $X = 0$, and (11) implies $f = g$. The boundary condition (52) on $X = 1$, on using (60)-(62), now yields the transport equation

$$U_p(\epsilon\bar{t}) + \Lambda \sin(2\pi\omega\bar{t}) = \epsilon^{-\frac{1}{2}} [f(\beta) - f(\alpha)] + \frac{1}{2\omega}(\beta - \alpha)P'_0(\sigma) + \frac{1}{3}\omega^2\kappa [f''(\beta) - f''(\alpha) - (\beta - \alpha)(f'''(\beta) + f'''(\alpha))]. \tag{64}$$

Equations (63) and (64) constitute a nonlinear differential-difference equation. Appealing to (34), (64) becomes

$$\Lambda \sin(2\pi\omega\bar{t}) = \epsilon^{-\frac{1}{2}} [f(\beta) - f(\alpha)] + \frac{1}{2\omega}(\beta - \alpha + 2\omega)P'_0(\sigma) + \frac{1}{3}\omega^2\kappa [f''(\beta) - f''(\alpha) - (\beta - \alpha)(f'''(\beta) + f'''(\alpha))]. \tag{65}$$

On iterating (63), and noting that, by (64), $f(\beta) = f(\alpha)$ to $O(\epsilon^{-\frac{1}{2}})$, (63) can be simplified to

$$\alpha = \beta + 2\omega - \frac{\epsilon^{\frac{1}{2}}}{1 + P_0(\sigma)} \left[F(\beta) + \frac{1}{2\omega} \int_{\beta}^{\beta+2\omega} F(s)ds \right], \tag{66}$$

where $F = 6\omega f$. This is the travel time equation. Then (66) implies that $(\beta - \alpha + 2\omega)P'_0(\sigma)$ is $O(\epsilon^{\frac{1}{2}})$, and thus negligible compared with the other terms in (65). We can contrast the role of the term $(\beta - \alpha + 2\omega)P'_0(\sigma)$ in (65), where it is negligible, with its role in (37). We now write (65) as

$$F(\alpha) = F(\beta) + \frac{1}{3}\omega^2\kappa\epsilon^{\frac{1}{2}} [F''(\beta) - F''(\alpha) + 2\omega (F'''(\beta) + F'''(\alpha))] + 6\omega\Lambda\epsilon^{\frac{1}{2}} \sin(2\pi\omega\bar{t}) + O(\epsilon). \tag{67}$$

Since $F(\alpha) = F(\beta) + O(\epsilon^{\frac{1}{2}})$, we rewrite (67) as

$$F(\alpha) = F(\beta) + \frac{4}{3}\omega^3\kappa\epsilon^{\frac{1}{2}}F'''(\beta) + 6\omega\Lambda\epsilon^{\frac{1}{2}} \sin(2\pi\omega\bar{t}) + O(\epsilon). \tag{68}$$

Our interest lies near the fundamental frequency $\omega = \frac{1}{2}$, and we thus set

$$\omega = \frac{1}{2}(1 + 2\epsilon^{\frac{1}{2}}\Delta), \tag{69}$$

where $\epsilon^{\frac{1}{2}}\Delta$ is the detuning. On calculating $F(\alpha)$ using (66) and equating to $F(\alpha)$ given by (68), we get, on noting (69), the nonlinear differential-difference equation

$$F(\beta + 1) = F(\beta) + \frac{4\omega^3}{3}\kappa\epsilon^{\frac{1}{2}}F'''(\beta) + 3\Lambda\epsilon^{\frac{1}{2}} \sin(2\pi\omega\bar{t}) - \epsilon^{\frac{1}{2}} \left[2\Delta - \frac{1}{1 + P_0(\sigma)} \left\{ F(\beta) + \int_{\beta}^{\beta+1} F(s)ds \right\} \right] F'(\beta + 1) + O(\epsilon). \tag{70}$$

As before we use a two time-scale expansion to reduce (70) to a partial differential equation. Let

$$F(\beta; \epsilon) = F_0(\beta, \tau) + \epsilon^{\frac{1}{2}}F_1(\beta, \tau) + \dots, \tag{71}$$

where the ‘slow’ time variable is $\tau = \epsilon^{\frac{1}{2}}\beta$. Substituting into (70) we get

$$F_0(\beta + 1, \tau) - F_0(\beta, \tau) = 0, \tag{72}$$

and

$$F_1(\beta + 1, \tau) - F_1(\beta, \tau) = 3\Lambda \sin(2\pi\omega\bar{t}) - \frac{\partial F_0}{\partial \tau} + \frac{4\omega^3}{3}\kappa \frac{\partial^3 F_0}{\partial \beta^3} - \left[2\Delta - \frac{1}{1 + P_0(\sigma)} \{F_0 + M_0(\tau)\} \right] \frac{\partial F_0}{\partial \beta}, \tag{73}$$

where

$$M_0(\tau) = \int_{\beta}^{\beta+1} F_0(s, \tau)ds$$

is the mean of F_0 over one cycle. Thus, by (72), F_0 is a standing wave, or free oscillation, with unit period in β , which is modulated on the longer time scale

associated with τ . The signal $F_0(\beta, \tau)$ is determined by avoiding resonance in (73), and thus requiring

$$\frac{\partial F_0}{\partial \tau} + \left[2\Delta + \frac{1}{1 + P_0(\sigma)} \{F_0 + M_0(\tau)\} \right] \frac{\partial F_0}{\partial \beta} - \frac{4}{3} \omega^3 \kappa \frac{\partial^3 F_0}{\partial \beta^3} = 3\Lambda \sin(2\pi\omega\bar{t}). \tag{74}$$

The completion of the partial differential equation (74) requires that $\omega\bar{t}(\alpha, \beta)$ on $X = 1$ be written in terms of β and τ . In direct analogy with (23),

$$\omega\bar{t}(\alpha, \beta) = \epsilon^{-1} \int_{\epsilon}^{\frac{1}{2}\epsilon(\alpha+\beta)} [1 + P_0(s)]^{-3} ds + O(\epsilon). \tag{75}$$

Then, as in Cox et al [7],

$$\omega\bar{t}(\alpha, \beta) = \beta + \frac{1}{2} + \frac{3}{2}\epsilon U_p(0) \left(\beta + \frac{1}{2}\right)^2 + \dots, \tag{76}$$

where time is measured from the onset of resonance at the wavelet labelled $\tilde{\beta} = 0$. On noting (69), the definition of τ , and $\Lambda = \pi/2$, (74) becomes

$$\begin{aligned} \frac{\partial F_0}{\partial \tau} + \left[2\Delta - \frac{1}{1 + P_0(\sigma)} \{F_0 + M_0(\tau)\} \right] \frac{\partial F_0}{\partial \beta} - \frac{\kappa}{6} \frac{\partial^3 F_0}{\partial \beta^3} \\ = \frac{3\pi}{2} \sin 2\pi \left(\beta + \frac{3}{2} U_p(0) \tau^2 \right). \end{aligned} \tag{77}$$

If we integrate (77) with respect to β over one period (unity) we find

$$M_0(\tau) = M_0(0)$$

which can be set equal to zero by a redefinition of the reference state. Also $|\beta| \leq O(\epsilon^{\frac{1}{2}})$ in the resonant band and thus $P_0(\sigma) \approx P_0(0) + O(\epsilon^{\frac{1}{2}})$ there. In our numerical solutions we consequently set $P_0(\sigma)$ to zero. It is for this reason that equations (58) and (59) have a relatively simple form and the term $(1 + P_0(\sigma))^6$ does not occur.

Equation (77) is a forced KdV equation where the ‘periodic’ forcing has a slowly varying frequency. If we set $\kappa = 0$ in (77), we reduce to the case of a polytropic gas with $\gamma = 2$ and recover the results of Steinruck [15] and Cox et al [7].

If we compare the left hand sides of equations (42) and (77), we notice that the term involving $P'_0(\tau)$ is missing from (77). This follows from the fact that $(\beta - \alpha + 2\omega)P'(\sigma)$ is negligible compared to other terms in (65), which is not the case with $(\alpha - \beta - 2)P'_0(\sigma)$ in (37). The timescale on which the forcing term sweeps through the resonant band is not sufficient for the expansion or contraction of the tank to have an effect on the fluid motion other than changing the frequency of the forcing term.

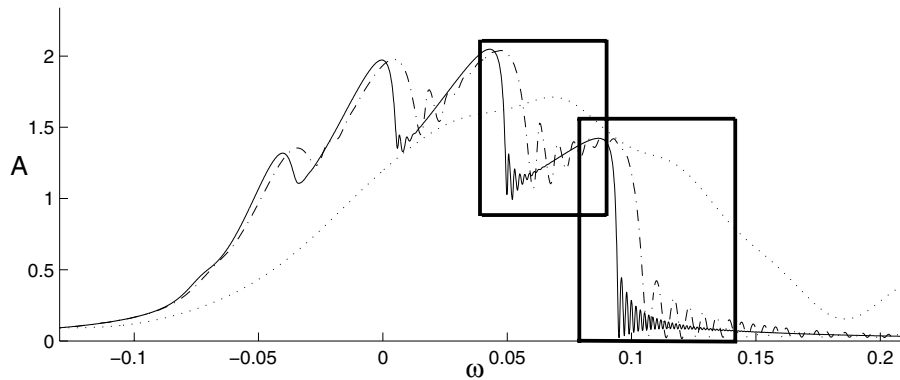


Figure 13. Response curves for positive $U_p(0)$ values: $U_p(0) = 0.7$ (dotted), $U_p(0) = 0.044$ (dot-dash), $U_p(0) = 0.011$ (solid)

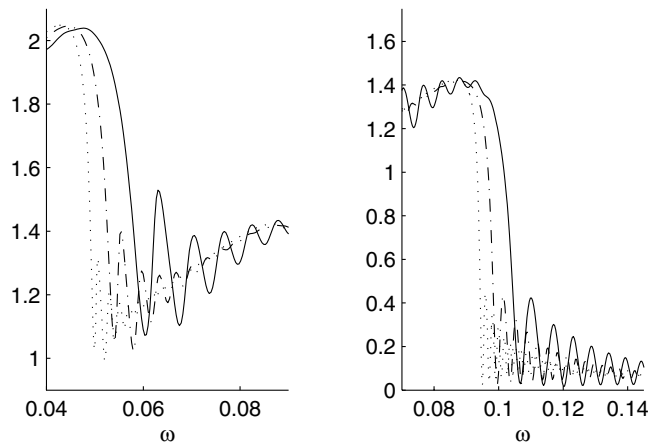


Figure 14. Closer views of the jumps highlighted in Figure 13: here, $U_p(0)$ has values 0.044 (solid), 0.022 (dot-dash), and 0.011 (dotted)

4.1. Numerical results for passage through resonance

Equation (77), which describes how a developed signal changes as the applied frequency moves through the resonant band, is the equivalent of equation (4.3) in Cox and Mortell [6], the significant difference being the presence of the term $3/2U_p(0)\tau^2$ within the argument of the forcing term in (77). With $\kappa = 0$, (77) also agrees with (5.26) in Cox et al [7] when $\lambda = 0$, i.e., it reduces to the undamped gas case. In this section we demonstrate some numerical solutions, obtained using a Fourier pseudospectral method in the periodic β direction, and a fourth-order Runge-Kutta method in time τ . Fast Fourier Transform techniques are utilised for efficient evaluation of nonlinear terms. Damping is included in the equations via

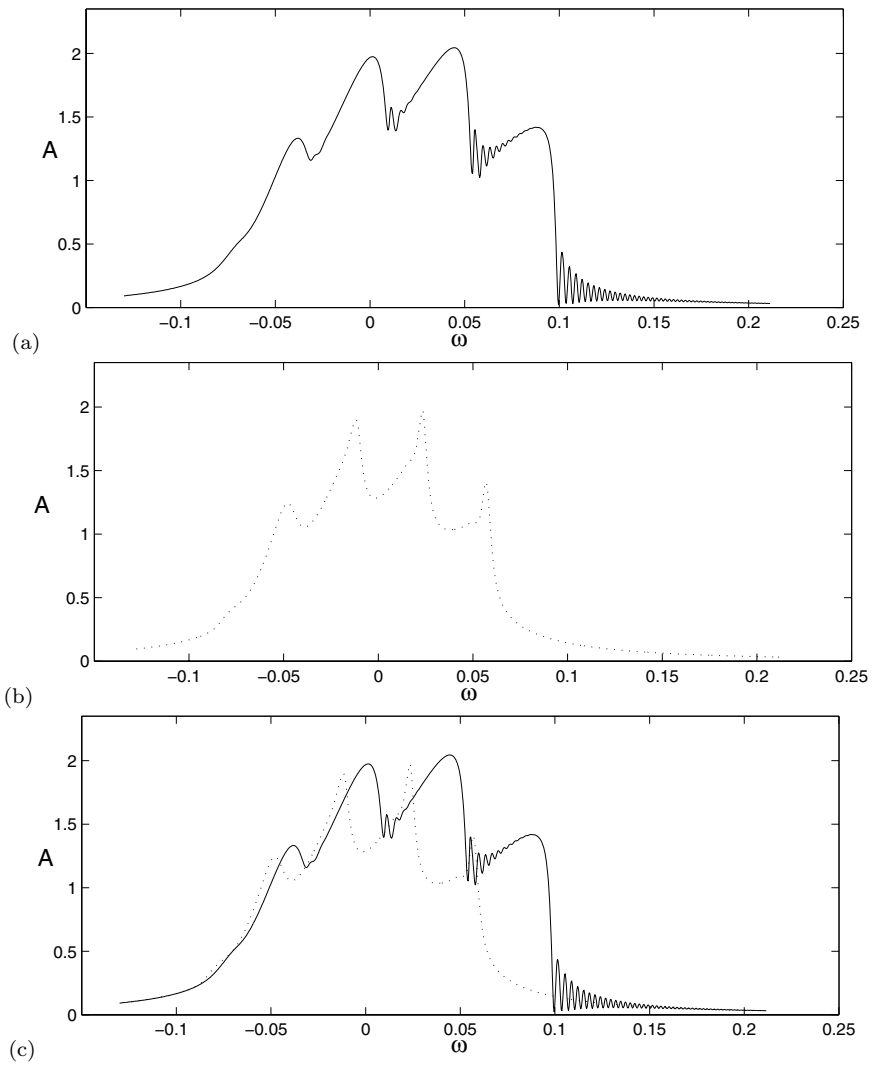


Figure 15. Response curves for $U_p(0) = 0.022$, moving (a) from left to right, and (b) from right to left. Plot (c) is a superposition of (a) and (b) to show the branch structures.

an extra Burgers term with coefficient a on the right hand side, and note the use of the forcing frequency parameter n_f ($n_f = 1$ gives the fundamental resonance, $n_f = 3/2$ gives the first overtone):

$$\begin{aligned} \frac{\partial F_0}{\partial \tau} + \left[2\Delta - \frac{1}{1 + P_0(\sigma)} \{F_0 + M_0(\tau)\} \right] \frac{\partial F_0}{\partial \beta} - \frac{\kappa}{6} \frac{\partial^3 F_0}{\partial \beta^3} \\ = a \frac{\partial^2 F_0}{\partial \beta^2} + \frac{3\pi}{2} \sin 2\pi \left(n_f \beta + \frac{3}{2} U_p(0) \tau^2 \right). \end{aligned} \quad (78)$$

The periodic and initial conditions are

$$F_0(\beta + 1, \tau) = F_0(\beta, \tau) \text{ and } F_0(\beta, 0) = 0. \quad (79)$$

We use this equation to examine the structure of solutions in the frequency bands about the fundamental and first overtone, and compare our results with the experimental observations in Chester and Bones [4].

Figure 13 shows the response (amplitude–frequency) curve, A - ω curve, around the fundamental frequency (normalised to $\omega = 0$). The measure of the amplitude of the response, $A(\tau)$, is given by

$$A(\tau) = 2 \int_0^1 [F_0(\beta, \tau)]^2 d\beta. \quad (80)$$

The parameters $a = 4.5 \times 10^{-3}$, $\kappa = 5.937 \times 10^{-3}$ are chosen to closely match Figure 14 of Chester and Bones [4]. The passage through the fundamental resonance in the A - ω plane begins with a resonant signal at $\tau = 0$ at detuning $\omega = -0.13$ ($\Delta = -0.9$) and moves to the right with various “speeds” determined by $U_p(0)$. At relatively fast speeds such as $U_p(0) = 0.7$ (dotted line in Figure 13), no real structure is discernible, but as we move more slowly from left to right ($U_p(0) = 0.044$ for the dot-dash curve, and $U_p(0) = 0.022$ for the solid curve), we note a 4-branch structure, with the solution amplitude jumping down from one branch to the next as the effective driving frequency increases. After each jump, the amplitude oscillates before reaching an equilibrium. We examine two of the jumps more closely in Figure 14, concentrating on the slower speeds, so here the $U_p(0)$ values are 0.044 (solid curve), 0.022 (dot-dash) and 0.011 (dotted). Note that there are oscillations after the jump downwards: for slower $U_p(0)$ these oscillations, which initially are of similar amplitudes, attenuate more quickly.

For definiteness we now concentrate on the $U_p(0) = \pm 0.022$ case. The response curve found by moving from left to right is reproduced in Figure 15(a), and that resulting from moving right to left (beginning with detuning $\omega = 0.2116$) is given by a dotted line in Figure 15(b). By superposing these plots (Figure 15(c)), the structure of the four solution branches may be seen. Figure 16 provides a stylized sketch of the four-branch structure, ignoring all oscillations, with the branches accessed by moving left to right drawn with solid line segments, and dashed lines used for those branches accessed by moving right to left. Of course we can only access the stable parts of each branch and so cannot show the unstable parts

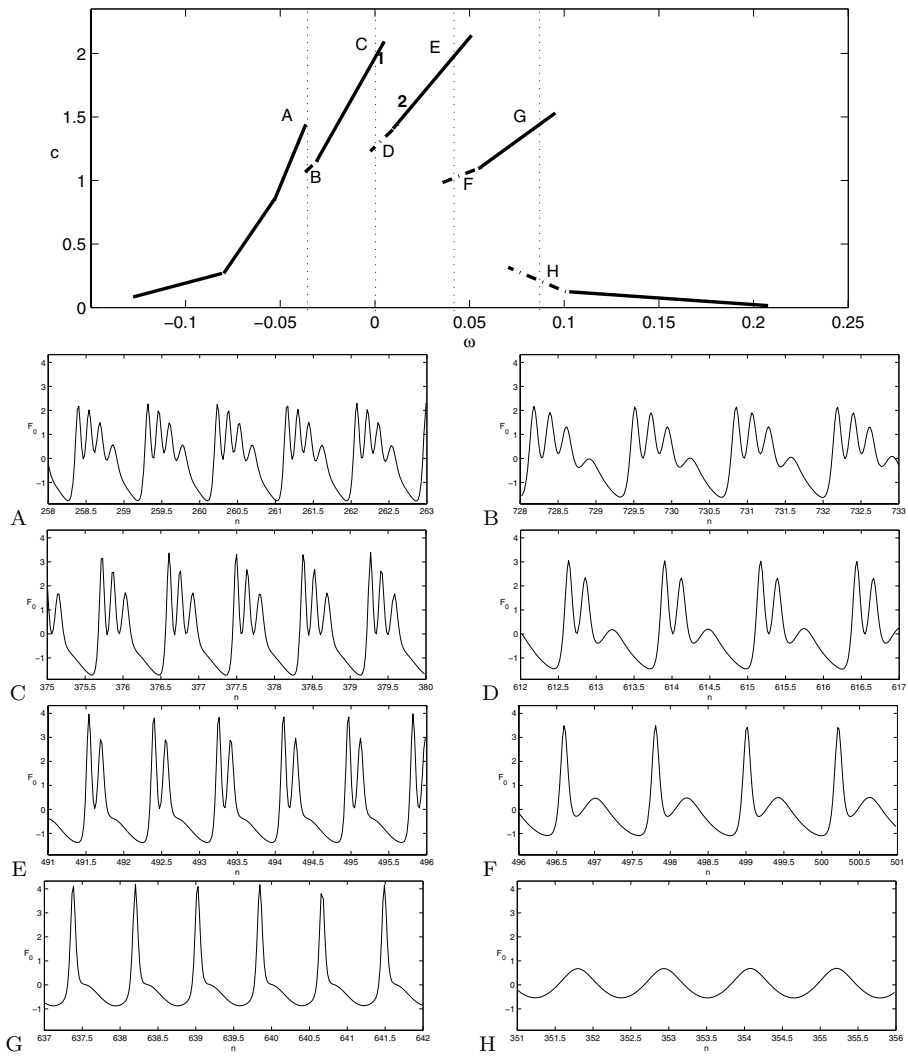


Figure 16. Branches and associated solutions over five periods of the forcing.

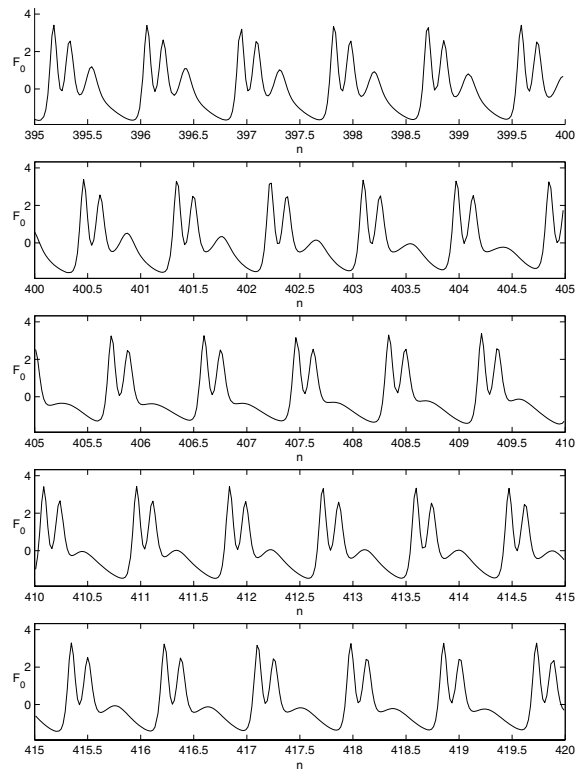


Figure 17. Soliton loss in moving from point 1 to point 2 in Figure 16.

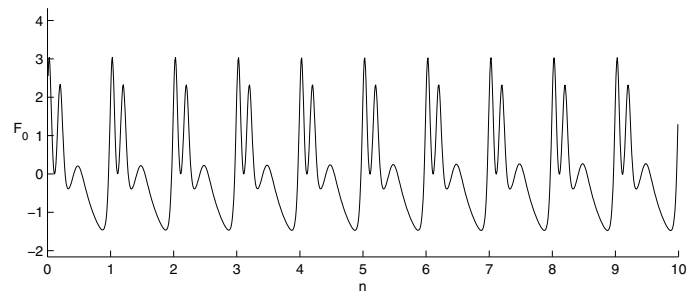


Figure 18. Steady periodic solution (10 periods) at $\omega = 0$, corresponding to point D in Figure 16; diffusion coefficient $a = 4.5 \times 10^{-3}$.

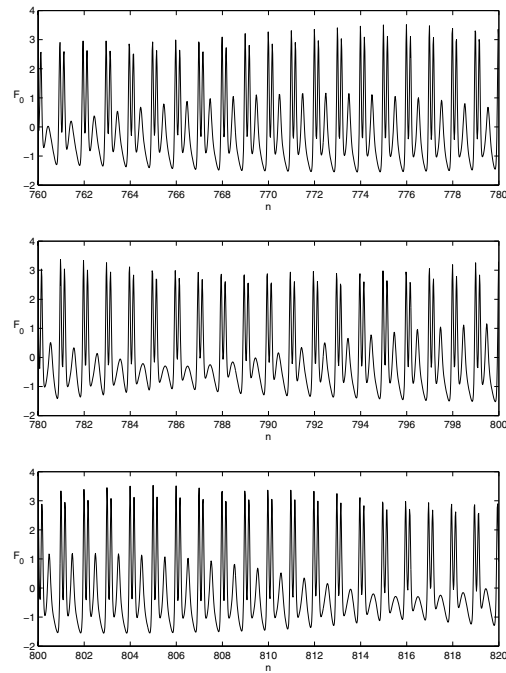


Figure 19. Unsteady beating solution (60 periods of forcing) at $\omega = 0$; diffusion coefficient $a = 1.8 \times 10^{-3}$.

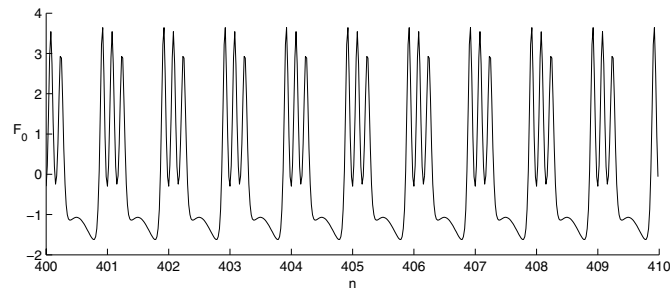


Figure 20. Steady periodic solution (10 periods) at $\omega = 0$, corresponding to point C in Figure 16; diffusion coefficient $a = 1.5 \times 10^{-3}$.

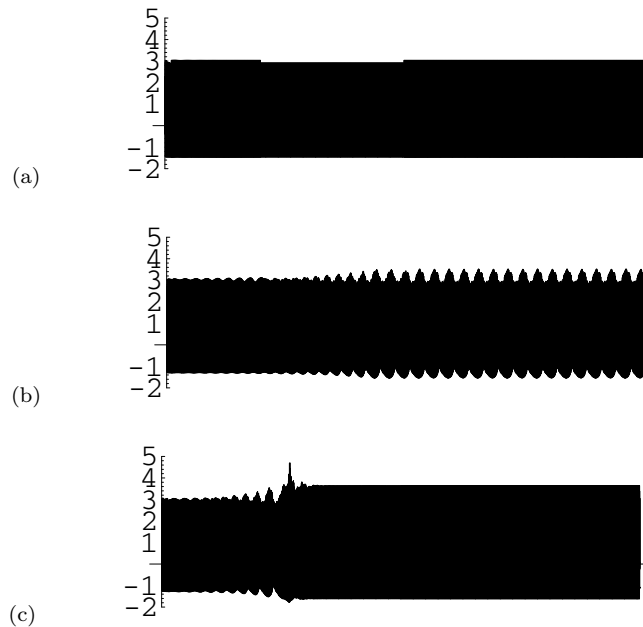


Figure 21. Long-time (960 forcing periods) evolution of solutions at $\omega = 0$ for diffusion coefficient values: (a) $a = 4.5 \times 10^{-3}$, (b) $a = 1.8 \times 10^{-3}$, (c) $a = 1.5 \times 10^{-3}$.

that would give a closed curve structure. The pairs of letters (A,B), (C,D), etc. are used to label positions on the response curve where multiple solutions exist for particular values of ω , depending on the initial conditions. For instance, at $\omega = 0$, the upper branch solution is shown as C (note the three solitons per forcing period), whereas the lower branch solution (accessed by moving from right to left) is shown in D, and has only two main solitons. Beginning from the left (at the point marked A), we note that at each jump downwards a soliton peak is lost until eventually the linear solution is reached near a detuning of 0.1. The results given here agree with Chester and Bones [4]; see their Figure 14. In order to examine the process of soliton loss, we display in Figure 17 the evolution of the signal corresponding to moving from the point marked 1 on Figure 16 to the point 2. A jump downward on the response curve is seen to correspond to the loss of one soliton peak.

As noted in Cox and Mortell [6], beating solutions may be found for certain parameter values. Moving from right to left with $U_p(0) = -0.022$ (i.e. along the curve in Figure 15(b)) to $\omega = 0$ and then setting $U_p(0) = 0$ allows us to examine the long-term behaviour of solutions corresponding to the point D in Figure 16. With the Burgers' diffusion coefficient $a = 4.5 \times 10^{-3}$ as above, the steady periodic two-soliton solution shown in Figure 18 is found. As expected,

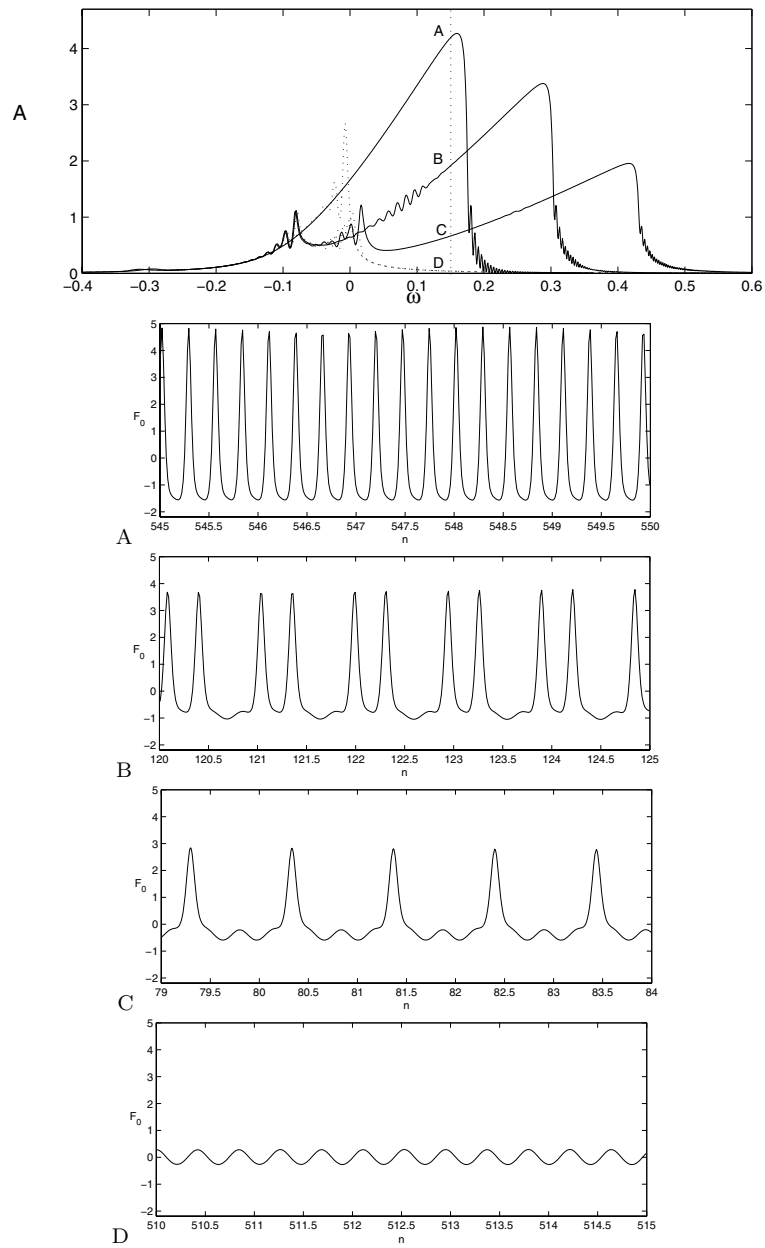


Figure 22. Response curve and associated subharmonic solutions at $\omega = 0.15$ over five periods of forcing, near second resonant frequency.

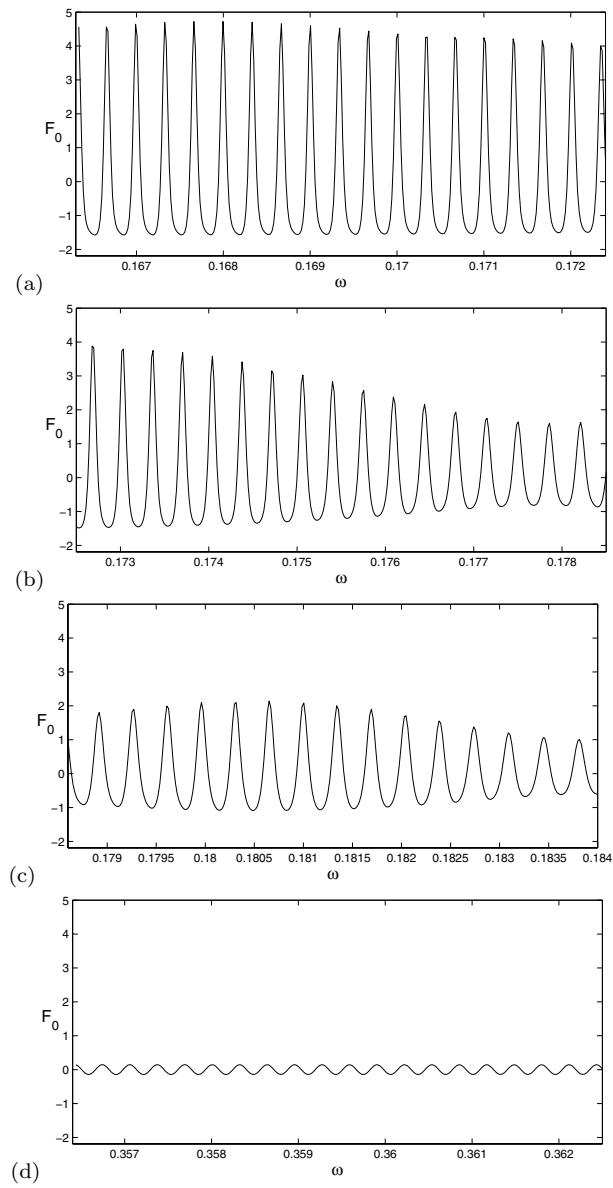


Figure 23. Evolving signal at various effective frequencies ω , moving from left to right along the curve marked A in Fig. 22.

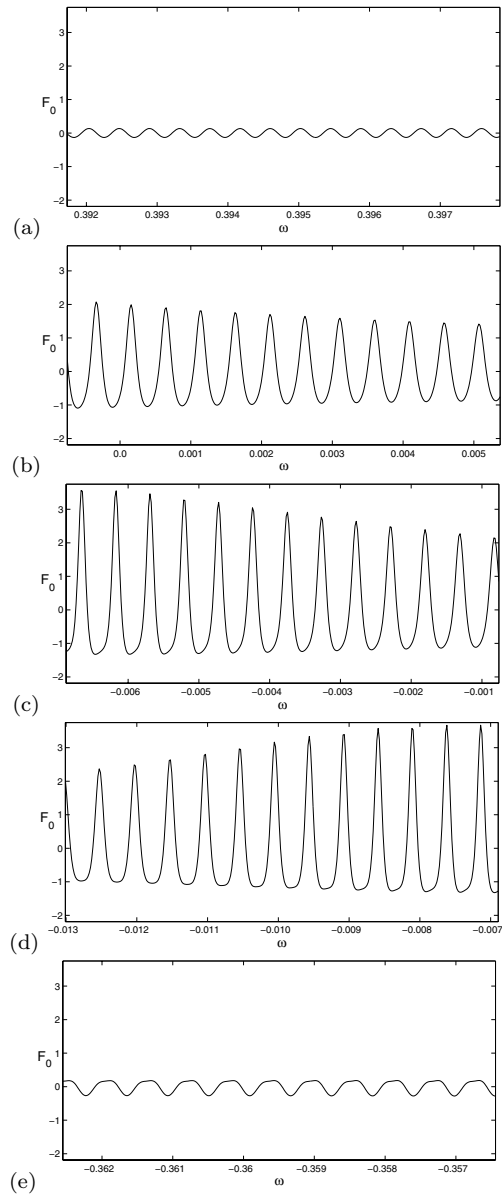


Figure 24. Evolving signal at various effective frequencies ω , moving from right to left along dotted curve in Fig. 22.

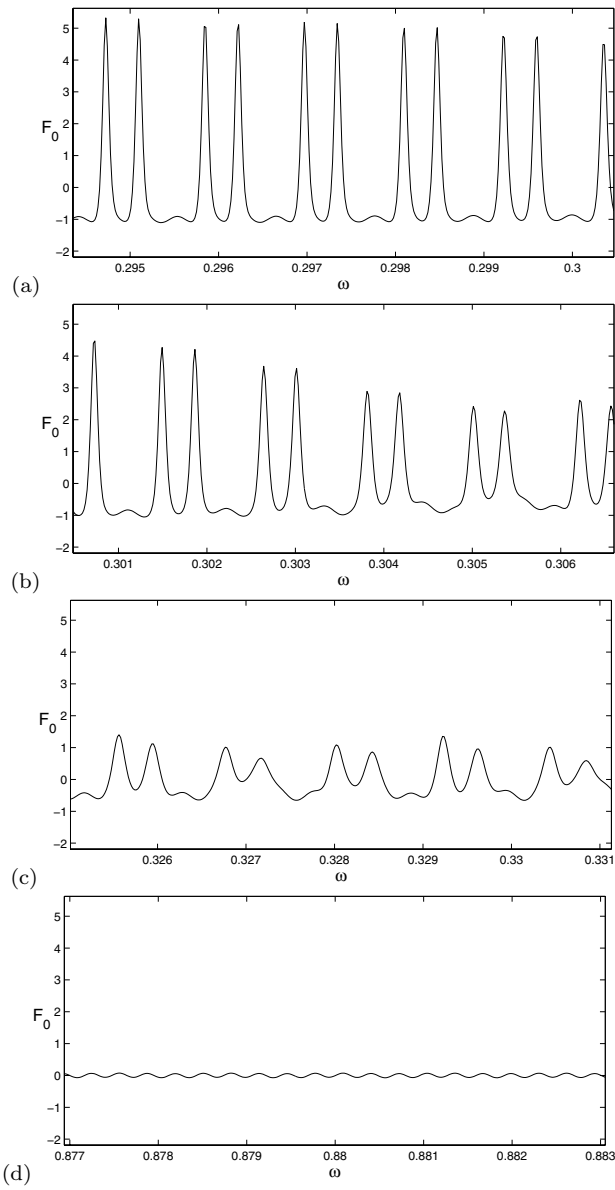


Figure 25. Evolving signal at various effective frequencies ω , moving from left to right along the curve marked B in Fig. 22.

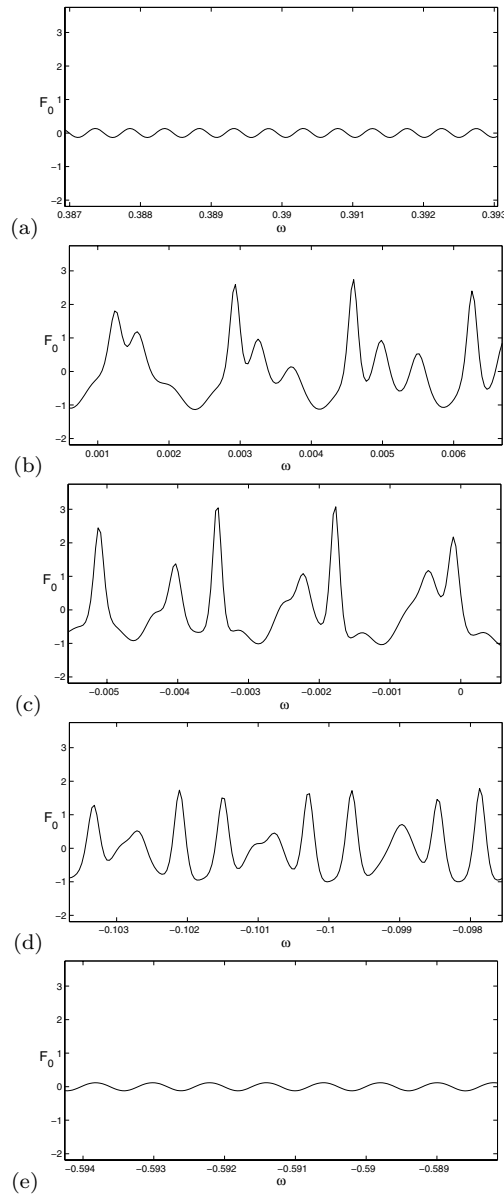


Figure 26. Evolving signal at various effective frequencies ω , moving from right to left, starting from the initial condition given by Fig. 25(d).

this has the same form as Figure 16 D (lower branch). However repeating the entire procedure with a lower diffusion coefficient of $a = 1.8 \times 10^{-3}$ leads not to a steady periodic solution, but rather to a beating solution, which appears to persist indefinitely. Figure 19 shows the beating solution over 60 periods of the forcing - the beat period is approximately 30 times the forcing period. Note the beating is largely due to the periodic growth and decay of the third soliton-like structure. The same procedure with an even lower diffusion value $a = 1.5 \times 10^{-3}$ is again found to yield a periodic steady state, albeit after a rather long transient time (on the order of 200 forcing periods). This periodic state is shown in Figure 20, and clearly corresponds to the upper branch solution, i.e. point C of Figure 16. The long-time evolution of the solutions is compared in Figure 21 for the three diffusion levels already discussed. Each case is plotted over 960 forcing periods, so only the envelope of beats over long time scales is visible. For $a = 4.5 \times 10^{-3}$, the steady periodic solution shows a constant envelope (Fig. 21a), which corresponds to the lower branch solution. At $a = 1.8 \times 10^{-3}$, however, the beating effect is clearly visible (Fig. 21b), whereas for $a = 1.5 \times 10^{-3}$, the upper branch periodic solution is eventually attained (Fig. 21c). We thus are led to an interpretation of the beating phenomenon as a tension between the two possible periodic states at C and D, with the Burgers' diffusion coefficient playing the role of a critical parameter. We note that similar dependence on the Burgers' diffusion coefficient may be demonstrated for the beating example shown in [6].

Figure 22 is the response curve centred around the second resonant frequency (first overtone). The parameters are $a = 0.01$, $\kappa = 5.137 \times 10^{-3}$, and $n_f = 3/2$. There are four branches in the response curve, and the four stable oscillations near $\omega = 0.15$ are displayed in Figure 22. Note that each branch supports a different number of solitons per period of the forcing. The solid response curve marked as A is found by initializing at $\omega = -0.2776$, and moving right, i.e. increasing the effective frequency, with $U_p(0) = 0.059$. Samples of the evolution of the signal are shown in Fig. 23. Each graph is over five forcing periods as before, but is now labelled by the equivalent frequency to facilitate comparison with Fig. 22. Note the decay in amplitude of oscillation near $\omega = 0.175$ (Fig. 23(b)), corresponding to the decay of the response amplitude clearly visible in Fig. 22. Eventually a linear response level is reached (Fig. 23(d)).

Next, we begin anew by using the linear-level response shown in Fig. 23(d) as our initial condition, and reverse direction, taking $U_p(0) = -0.059$. The response curve is the dotted line in Fig 22, with an upward jump to the top branch near $\omega = 0$. The corresponding evolution is shown in Fig. 24.

To reach the subharmonic response curve marked as B in Fig. 22, it is necessary to "seed" the initial condition as follows. Taking the three-peak (top branch) solution at $\omega = 0$, we erase one peak, and use this as the initial condition to generate a new equilibrium solution (holding $U_p(0) = 0$). Then this equilibrium solution is evolved (with $U_p(0) = 0.059$) to generate the response curve marked as B. Examples of the evolution of the signal as the effective frequency is increased

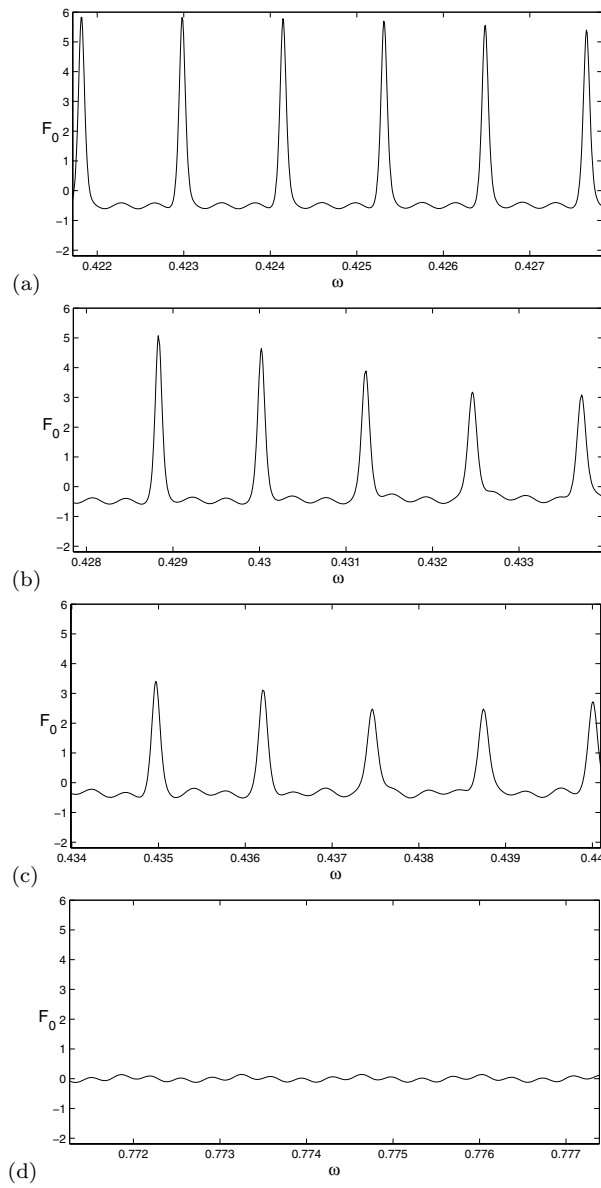


Figure 27. Evolving signal at various effective frequencies ω , moving from left to right along the curve marked C in Fig. 22.

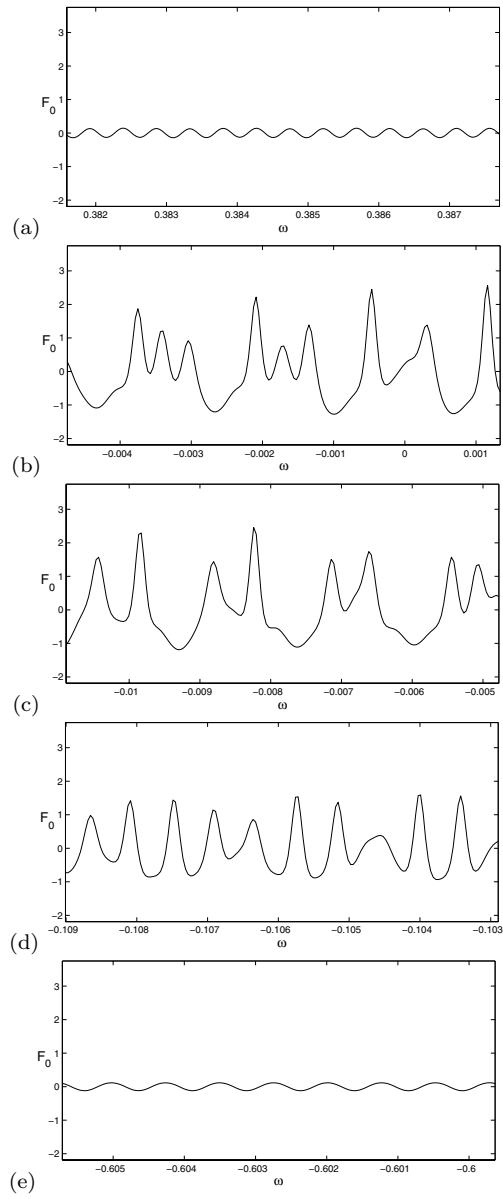


Figure 28. Evolving signal at various effective frequencies ω , moving from right to left, starting from the initial condition given by Fig. 27(d).

are shown in Fig. 25; note the decay in amplitude near $\omega = 0.3$. Having evolved this solution until it reaches the linear regime (Fig. 25(d)), we again reverse the direction of motion, setting $U_p(0) = -0.059$, and generate the lower dotted line response curve in Fig 22. Again, examples of evolution along this curve are shown in Fig. 26.

The branch marked C has one soliton peak per period (Fig. 22) and is found by erasing two peaks from the three-peak solution and evolving to equilibrium at $\omega = 0.25$. Further evolution with $U_p(0) = 0.059$ defines the response branch C in Fig. 22, with evolution towards the linear-level state shown in Fig. 27. Reversing the direction (i.e., setting $U_p(0) = -0.059$) with the linear-level state as initial condition leads to the dotted response curve shown in Fig. 22 – this is practically indistinguishable from that resulting from the B branch and displays a similar evolution: compare Fig. 28 and Fig. 26.

The stable oscillations with two peaks (branch B) and one peak (branch C) per period of forcing are called “subharmonics” by Chester and Bones [4]. The response curves shown here are in close accord with Figure 17 of Chester and Bones [4].

5. Conclusion

In summary, we have derived equations describing resonantly slowly changing forced oscillations and slowly changing nonlinear standing waves of the water surface in a closed tank. Numerical solutions show that the number of solitons in the tank changes as the tank length is (slowly) altered; moreover, the number of solitons is shown to depend not only on the instantaneous length, but on its time-history. In considering passage through resonance we demonstrated the existence of amplitude-frequency response curves with multiple branches, as found experimentally by Chester and Bones [4]. Beating solutions found in the experiments, and reproduced in Cox and Mortell [6], are shown to exist between two different periodic steady states, with the damping parameter playing a crucial role.

Acknowledgements

The work of JPG is funded by a Science Foundation Ireland Investigator Award, programme number 02/IN.1/IM062.

References

- [1] D. E. Amundsen, E. A. Cox, M. P. Mortell, S. Reck, Evolution of nonlinear sloshing in a tank near half the fundamental resonance, *Studies in Applied Mathematics* **107** (2001), 103–125.
- [2] R. Betchov, Nonlinear oscillations of a column of gas, *Phys. Fluids*, **1** (1958), 205–212.

- [3] W. Chester, Resonant oscillations of water waves I. Theory, *Proc. R. Soc. Lond. A* **306** (1968), 5–22.
- [4] W. Chester and J. A. Bones, Resonant oscillations of water waves II. Experiment, *Proc. R. Soc. Lond. A* **306** (1968), 23–39.
- [5] E. A. Cox and M. P. Mortell, The evolution of resonant oscillations in closed tubes, *Z. Angew. Math. Phys. (ZAMP)* **34** (1983), 845–866.
- [6] E. A. Cox and M. P. Mortell, The evolution of resonant water-wave oscillations, *J. Fluid Mech.* **162** (1986), 99–116.
- [7] E. A. Cox, M. P. Mortell and S. Reck, Nonlinear standing and resonantly forced oscillations in a tube with slowly changing length, *SIAM J. Appl. Math.* **62** (2002), 965–989.
- [8] R. A. Ibrahim, V. N. Pilipchuk and T. Ikeda, Recent advances in liquid sloshing dynamics, *Appl. Mech. Rev.* **54** (2001), 133–199.
- [9] R. Klein and N. Peters, Cumulative effects of weak pressure waves during the induction period of a thermal explosion in a cylinder, *J. Fluid Mechanics* **187** (1988), 197–230.
- [10] C. C. Lin, On a perturbation method based on the method of characteristics, *J. Math. Phys.* **33** (1954), 117–134.
- [11] M. P. Mortell, The evolution of nonlinear standing waves in bounded media, *Z. Angew. Math. Phys. (ZAMP)* **28** (1977), 33–46.
- [12] M. P. Mortell and E. Varley, Finite amplitude waves in bounded media: nonlinear vibrations of an elastic panel. *Proc. R. Soc. Lond. A* **318** (1970), 169–196.
- [13] A. Salupere, G. A. Maughin, J. Engelbrecht and J. Kalda, On the KdV soliton formation and discrete spectral analysis, *Wave Motion* **23** (1996), 49–66.
- [14] B. R. Seymour, and M. P. Mortell, Resonant acoustic oscillations with damping: small rate theory, *J. Fluid Mech.* **58** (1973), 353–373.
- [15] H. Steinruck, The passing of resonant zones of a piston in a closed tube, *Z. Angew. Math. Mech. (ZAMM)* **75** (1995), 223–232.
- [16] G. B. Whitham, *Linear and Nonlinear Waves*, John Wiley and Sons, New York 1974.
- [17] N. J. Zabusky and M. D. Kruskal, Interactions of “solitons” in a collisionless plasma and the recurrence of initial states, *Phys. Rev. Lett.* **15** (1965), 240–243.

E. A. Cox
Dept. of Mathematical Physics
University College
Dublin
Ireland

J. P. Gleeson and M. P. Mortell
Dept. of Applied Mathematics
University College
Cork
Ireland

(Received: December 16, 2003)



To access this journal online:
<http://www.birkhauser.ch>
